Landau level collapse in graphene in the presence of in-plane radial electric and perpendicular magnetic fields

I. O. Nimyi,[1,2] V. Könye,[2] S. G. Sharapov,[3,1] and V. P. Gusynin[3]
[1]*Kyiv Academic University, 03142 Kyiv, Ukraine*
[2]*Institute for Theoretical Solid State Physics, IFW Dresden and Würzburg-Dresden Cluster of Excellence ct.qmat, Helmholtzstr. 20, 01069 Dresden, Germany*
[3]*Bogolyubov Institute for Theoretical Physics, National Academy of Science of Ukraine, 14-b Metrologichna Street, Kyiv, 03143, Ukraine*

(Received 8 June 2022; accepted 21 July 2022; published 2 August 2022)

It is known that in two-dimensional relativistic Dirac systems placed in orthogonal uniform magnetic and electric fields, the Landau levels collapse as the applied in-plane electric field reaches a critical value $\pm E_c$. We study this phenomenon for a distinct field configuration with in-plane constant radial electric field. The Dirac equation for this configuration does not allow analytical solutions in terms of known special functions. The results are obtained by using both the WKB approximation and the exact diagonalization and shooting methods. It is shown that the collapse occurs for positive values of the total angular momentum quantum number, the hole (electron)-like Landau levels collapse as the electric field reaches the value $+(-)E_c/2$. The investigation of the Landau level collapse in the case of gapped graphene shows a number of distinctive features in comparison with the gapless case.

DOI: 10.1103/PhysRevB.106.085401

I. INTRODUCTION

It was Rabi [1] who solved the just-discovered Dirac equation in a homogeneous magnetic field in the symmetric gauge and showed that the energies of the free electrons are quantized. This occurred two years before the corresponding quantized levels were found in the nonrelativistic quantum theory by Frenkel and Bronstein [2] and Landau [3]. However, the experimental exploration of the relativistic Landau levels, in contrast to the nonrelativistic ones, in condensed matter systems became possible almost 80 years later after the discovery of graphene [4,5]. Naturally, the most exciting are the properties of the relativistic Landau levels that do not have their counterparts for standard electron systems and among them is the Landau-level collapse phenomenon predicted in Ref. [6] (see also Ref. [7]) and observed experimentally in Refs. [8,9].

This phenomenon occurs when, in addition to a magnetic field H applied perpendicular to the sheet of graphene, an in-plane electric field E is present. It consists of the merging of the Landau-level staircase when the applied electric field reaches a critical value $\pm E_c$ with $E_c = (v_F/c)H$ in CGS units, where v_F is the Fermi velocity.

There are several ways to understand the origin of the collapse. The first one is based on the consideration of the motion in crossed electric and magnetic fields [10,11], where the motion of a quasiparticle having a dispersion $\mathcal{E}(\mathbf{p})$ in crossed fields can be viewed as a motion of a particle in the magnetic field only with the modified dispersion law,

$$\mathcal{E}^*(\mathbf{p}) = \mathcal{E}(\mathbf{p}) - \mathbf{v}_0\mathbf{p}, \tag{1}$$

with $\mathbf{v}_0 = c\mathbf{E}\times\mathbf{H}/H^2$ being the drift velocity for the motion in the crossed fields. Then the quasiclassical spectrum follows from the Lifshitz-Onsager quantization condition,

$$S(\mathcal{E}^*) = 2\pi\hbar\frac{eH}{c}(n+\gamma_B), \quad n = 0, 1, \ldots, \tag{2}$$

where $S(\mathcal{E}^*)$ is the electron orbit area in the momentum space, γ_B is the topological part of the Berry phase. For the quadratic dispersion law $\mathcal{E} = p^2/(2m)$ with m being the effective mass and p the absolute value of the momentum, the area is $S(\mathcal{E}^*) = 2\pi m\mathcal{E}^*$. Thus, one can see that in this case the electric field does not change the distance between Landau levels.

The massive Dirac fermions with the dispersion $\mathcal{E} = \pm\sqrt{v_F^2p^2+\Delta^2}$ are characterized by the area $S(\mathcal{E}) = \pi(\mathcal{E}^2 - \Delta^2)/v_F^2$, where Δ is the gap in the quasiparticle spectrum. The Lifshitz-Onsager quantization condition Eqs. (2) results in the spectrum in the crossed fields [12]

$$\mathcal{E}_n = \mathcal{E}_n^* - \hbar k\frac{E}{H},$$
$$\mathcal{E}_n^* = \pm(1-\beta^2)^{3/4}\sqrt{\frac{2n\hbar v_F^2eH}{c} + \frac{\Delta^2}{(1-\beta^2)^{1/2}}}, \tag{3}$$

where k is the in-plane wave vector along the direction perpendicular to the electric field, $\beta = v_0/v_F = cE/(v_FH)$, the phase $\gamma_B = 0$. For $\Delta = 0$, the spectrum Eqs. (3) reduces the spectrum obtained by an exact solution of the problem [6,7]. The Landau level collapse occurring at $|\beta| = 1$ can be viewed as a transition from the closed elliptic quasiparticle orbits for $|\beta| < 1$ ($|v_0| < v_F$) to open hyperbolic orbits for $|\beta| > 1$ ($|v_0| > v_F$) [13].

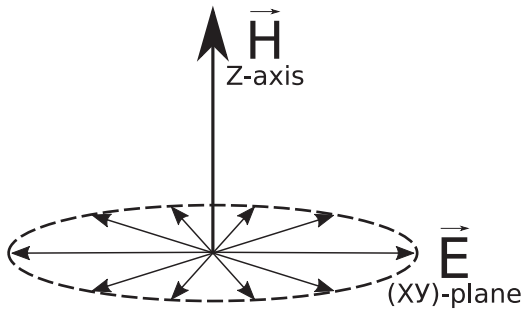

FIG. 1. Schematic figure for the electric and magnetic field configuration. The radial electric field E is in the plane of the graphene sheet and the uniform magnetic field H is perpendicular to this plane.

Another elegant way to understand the origin of the collapse and even to derive the spectrum Eqs. (3) is described in Ref. [6] (see also Refs. [13,14]). One can employ the effective Lorentz covariance of the equation of motion [see Eq. (8) below], in which the graphene dispersion velocity v_F plays the role of the speed of light c, and consider the corresponding Lorentz transformations for electromagnetic fields.

We assume that the magnetic and electric fields are directed in the z and y directions, respectively. Then under a boost in the x direction with velocity v, these fields transform as [15]

$$E_y' = \gamma\left(E_y - \frac{v}{c}H_z\right), \tag{4a}$$

$$H_z' = \gamma\left(H_z - \frac{vc}{v_F^2}E_y\right), \tag{4b}$$

where $\gamma = 1/\sqrt{1 - v^2/v_F^2}$. When the velocity v coincides with the drift velocity $v_0 = cE/H$ in graphene, the electric field disappears in the primed reference frame and the magnetic field becomes

$$H_z' = \sqrt{1-\beta^2}H. \tag{5}$$

Here we assumed that in the original frame $c|E| \leqslant v_F|H|$ (or $|\beta| \leqslant 1$). Since the Dirac equation is Lorenz covariant, the energies of Landau levels in the primed frame are known:

$$\mathcal{E}_n' = \pm\sqrt{2n\hbar v_F^2 eH_z'/c + \Delta^2}. \tag{6}$$

The value Δ/v_F^2 plays the role of the mass in the Dirac theory and remains invariant under Lorentz transformations. Considering that the energy is the zeroth component of the energy-momentum vector and doing the inverse boost transformation one recovers the spectrum Eq. (3). The critical value $|\beta| = 1$ corresponding to the collapse of all levels $\mathcal{E}_n^* = \mathcal{E}_n'\sqrt{1-\beta^2}$ is determined by the relationship Eq. (5) between H_z' and H.

The purpose of this paper is to study the Landau levels and their collapse in another field configuration with the magnetic field H applied perpendicular to the infinite graphene's plane and the in-plane constant radial electric field E as shown in Fig. 1. In practice, an approximately constant radial field can be created inside a cylindric capacitor, where the electric potential

$$V(r) = V_0 \ln\frac{r}{a} \approx V_0\left(\frac{r}{a} - 1\right), \quad b \leqslant r \leqslant a, \tag{7}$$

with a and b being the external and internal radii, respectively.

Unlike the above-described case of orthogonal uniform magnetic and electric fields, the present problem cannot be solved exactly in a closed analytic form. Thus, to investigate this problem, we employ the semiclassical WKB method which leads to a transcendental equation for the spectrum. These results are compared with the calculations performed using the exact diagonalization and shooting methods. It turns out that the WKB solutions are very close to the numerical ones for practically all quantum numbers.

Following the above-mentioned arguments with the Lorentz transformation, one may develop a qualitative understanding of the present problem. However, one should keep in mind that because the electric field is radial rather than unidirectional, the considered case rather resembles an explanation of the origin of spin-orbit interaction in atomic physics. Thus, the Thomas precession must be properly taken into account (see, for example, Ref. [16]). One can see from the transformation Eq. (4a) that by doing a boost to the coordinate system moving with the drift velocity $v_0 = cE/H$, it is possible to remove the electric field locally.

We emphasize that due to Thomas precession it is not sufficient to use the transformation Eq. (4b), and Eq. (5) has to be replaced by a more complicated unknown relationship $H_z' = \alpha(\beta)H$. The Landau-level collapse would still be possible if an unknown function $\alpha(\beta)$ goes to zero at some value of β. We later show that for the configuration of the fields in Fig. 1, $\beta = -1/2$ for electrons and $\beta = 1/2$ for holes.

The paper is organized as follows. In Sec. II, the model for a single layer of graphene with a magnetic field H applied perpendicular to the layer and an in-plane constant radial electric field is introduced. Using the symmetry of the problem, it is reduced to a system of radial equations. This system is considered using the WKB method in Sec. III. In particular, the transcendental WKB equation for the energy spectrum is derived in terms of complete elliptic integrals for gapless graphene. The technical details are provided in Appendices A and B. In the absence of an electric field, the WKB approximation recovers the exact solution as discussed both in Sec. III A and Appendix C. In Sec. IV, we obtain and discuss the energy spectra obtained in the WKB approximation and compare them with the results of numerical computations performed using the exact diagonalization and shooting methods. The gapped graphene case is considered using numerical methods in Sec. IV B. In the Conclusion (Sec. V), we summarize the obtained results and discuss their possible experimental observation.

II. MODEL AND MAIN EQUATIONS

We consider the stationary Dirac equation

$$[-\hbar v_F(\alpha_1 iD_x + \alpha_2 iD_y) + \Delta\alpha_3 + V(\mathbf{r}) - \mathcal{E}]\Psi(\mathbf{r}) = 0, \tag{8}$$

which describes low-energy excitations in graphene (see, e.g., Ref. [17] for a review and notations) and eigenenergy $\mathcal{E}$. The 4×4 α matrices $\alpha_i = \tau_3 \otimes \sigma_i$ and the Pauli matrices τ_i, σ_i (as well as the 2×2 unit matrices τ_0, σ_0) act on the valley ($\mathbf{K}_\eta$ with $\eta = \pm$) and sublattice (A, B) indices, respectively, of the four component spinors $\Psi^T = (\Psi_+^T, \Psi_-^T) = (\psi_{AK_+}, \psi_{BK_+}, \psi_{BK_-}, \psi_{AK_-})$.

We consider both the massless Dirac-Weyl fermions in the pristine graphene and the massive Dirac fermions with the

mass Δ. We recall that a global A/B sublattice asymmetry gap $2\Delta \sim 350$ K can be introduced in graphene [18–21] when it is placed on top of hexagonal boron nitride (G/hBN) and the crystallographic axes of graphene and hBN are aligned.

The orbital effect of a perpendicular magnetic field $\mathbf{H} = \nabla \times \mathbf{A}$ is included via the covariant spatial derivative $D_j = \partial_j + (ie/\hbar c)A_j$ with $j = x, y$ and $-e < 0$, while the potential $V(\mathbf{r})$ corresponds to the static electric field $e\mathbf{E} = \nabla V(\mathbf{r})$. The Zeeman interaction is neglected in this paper (see, e.g., Ref. [17]) and the spin index is omitted in what follows.

We consider the configuration of crossed magnetic and electric fields, with the magnetic field applied perpendicular to the infinite plane of graphene along the positive z axis [22] and the corresponding vector potential is taken in the symmetric gauge $(A_x, A_y) = (H/2)(-y, x)$ and radial in-plane electric field E with the potential $V(r) = eEr$ (see Fig. 1).

It is clear that the solution at the $\mathbf{K}_-$ point is obtained from the solution at the $\mathbf{K}_+$ point by changing $\Delta \to -\Delta$ and exchanging the spinor components $\psi_A \leftrightarrow \psi_B$, so in what follows we only consider the $\mathbf{K}_+$ point.

Since the system has rotational symmetry, it is natural to consider the problem in polar coordinates, where

$$iD_x \pm D_y = e^{\mp i\phi}\left(i\frac{\partial}{\partial r} \pm \frac{1}{r}\frac{\partial}{\partial \phi} \pm \frac{ieHr}{2\hbar c}\right). \tag{9}$$

Accordingly, the total angular momentum J_z is conserved and we can represent $\Psi(\mathbf{r})$ in terms of the eigenfunctions of $J_z = L_z + \sigma_z/2 = -i\partial/\partial\phi + \sigma_z/2$ as follows:

$$\Psi_+(\mathbf{r}) = \begin{bmatrix} e^{i(j-1/2)\phi} f(r) \\ ie^{i(j+1/2)\phi} g(r) \end{bmatrix}, \tag{10}$$

where $j = \pm 1/2, \pm 3/2, \ldots$ is the total angular momentum quantum number. Then for the spinor $\chi^T(r) = (f(r), g(r))$, we obtain the following system of equations written in a matrix form:

$$\chi'(r) = \frac{1}{\hbar} N(r)\chi(r), \tag{11}$$

where the prime denotes the derivative over r and the matrix

$$N = \begin{bmatrix} \frac{\hbar(j-1/2)}{r} + \frac{eHr}{2c} & -\frac{\mathcal{E}+\Delta-V(r)}{v_F} \\ \frac{\mathcal{E}-\Delta-V(r)}{v_F} & -\frac{\hbar(j+1/2)}{r} - \frac{eHr}{2c} \end{bmatrix}. \tag{12}$$

For a constant electric field with $V(r) = eEr$, one can rewrite the last equation in the form

$$\chi'(\rho) = N(\rho)\chi(\rho) = \left(\frac{A}{\rho} + B + C\rho\right)\chi(\rho), \tag{13}$$

where we introduced the dimensionless variable $\rho = r/l$ with $l = \sqrt{\hbar c/eH}$ being the magnetic length; the prime now denotes the derivative over ρ, and the 2×2 ρ-independent matrices A, B, C are, respectively,

$$A = \begin{bmatrix} j - 1/2 & 0 \\ 0 & -j - 1/2 \end{bmatrix},$$
$$B = \begin{bmatrix} 0 & -\frac{l(\mathcal{E}+\Delta)}{\hbar v_F} \\ \frac{l(\mathcal{E}-\Delta)}{\hbar v_F} & 0 \end{bmatrix},$$
$$C = \begin{bmatrix} 1/2 & \beta \\ -\beta & -1/2 \end{bmatrix}. \tag{14}$$

The matrix C contains the important dimensionless parameter $\beta = cE/(v_F H)$ that describes the strength of the electric field relative to the magnetic field. In this paper, we restrict ourselves to the $|\beta| \leqslant 1/2$ case.

Comparing the system of Eq. (13) with the corresponding system describing the Dirac fermions in the uniform magnetic field and constant electric field in the x direction [6,7] (see also Ref. [23]), one can see that the latter contains only two matrices $\tilde{B} + \tilde{C}x$. The problem in the crossed uniform fields in the Cartesian coordinates is exactly solvable by diagonalizing the matrix $\tilde{C}$, while the present problem with the radial electric field cannot be solved analytically. The situation is similar to the case of 2D Dirac fermions in a constant magnetic field and Coulomb potential (see, e.g., Refs. [24–28]) and to the parabolic potential $V(r) \sim r^2$ [29], which do not have analytical solutions in terms of known special functions.

Making in Eq. (13) the transformation of dependent variable $\chi(\rho) = U(\rho)\xi(\rho)$, where $U(\rho)$ is a 2×2 matrix with $\det U(\rho) \neq 0$, we obtain a different system of equations,

$$\xi'(\rho) = M(\rho)\xi(\rho), \tag{15}$$

with matrix $N(\rho)$ related to matrix $M(\rho)$ by the transformation

$$M(\rho) = U^{-1}(\rho)N(\rho)U(\rho) - U^{-1}(\rho)U'(\rho). \tag{16}$$

Choosing the matrix U proportional to the unit matrix $U = \sigma_0 e^{-a\rho^2/2}\rho^s$, one can see that matrix B does not change, while matrices A and C become

$$A = \begin{bmatrix} j - 1/2 - s & 0 \\ 0 & -j - 1/2 - s \end{bmatrix},$$
$$C = \begin{bmatrix} 1/2 + a & \beta \\ -\beta & -1/2 + a \end{bmatrix}. \tag{17}$$

Different sets of parameters a and s are appropriate for the consideration of the system Eq. (15), for example, choosing $a = 1/2$ and $s = -j - 1/2$ one obtains the following second-order differential equation for the lower component $\xi_2(\rho)$ of the spinor $\xi(\rho)$:

$$\xi_2'' - \left(\frac{2j}{\rho} + \rho + \frac{\beta}{\beta\rho - \epsilon + \delta}\right)\xi_2' + [(\beta\rho - \epsilon)^2 - \delta^2]\xi_2 = 0. \tag{18}$$

Here we introduced the dimensionless energy $\epsilon = l\mathcal{E}/(\hbar v_F)$, and mass (gap) $\delta = l\Delta/(\hbar v_F)$. This equation has three singular points, two regular at $\rho = 0$, $\rho = (\epsilon - \delta)/\beta$ and an irregular one at infinity. The singularity at $\rho = (\epsilon - \delta)/\beta$ is apparent [it is absent in the system Eq. (15)]. The equation is similar to the confluent Heun equation but the singularity at infinity is more strong (with rank three according to the definition of the rank of singular points of differential equations in Ref. [30]). The rank of the irregular singular point at infinity of the confluent Heun equation is equal to two. Analytical results for such type of equations are absent in the literature, thus it is necessary to use another method to investigate the problem.

III. WKB METHOD

We employ the WKB method to study the spectrum of bound states for the problem described by Eqs. (15) and (17). It is convenient to choose the exponent $s = -1/2$ and

$a = 0$ in Eqs. (17), so the spinor $\xi(r) = \sqrt{r}\chi(r)$. Restoring the dimensional variables, we rewrite Eq. (15) as follows:

$$\xi'(r) = \frac{1}{\hbar} M \xi(r), \tag{19}$$

where the matrix

$$M = \begin{bmatrix} \frac{J}{r} + \frac{eHr}{2c} & -\frac{\mathcal{E}+\Delta-V(r)}{v_F} \\ \frac{\mathcal{E}-\Delta-V(r)}{v_F} & -\frac{J}{r} - \frac{eHr}{2c} \end{bmatrix} = \frac{\hbar}{l} \begin{bmatrix} \frac{j}{\rho} + \frac{\rho}{2} & \beta\rho - \epsilon - \delta \\ -(\beta\rho - \epsilon + \delta) & -\frac{j}{\rho} - \frac{\rho}{2} \end{bmatrix}. \tag{20}$$

Here we denoted $J = \hbar j$ in the first line. Equations (19) and (20) are similar to the corresponding system written in Refs. [24,26–29] (see Ref. [22]).

As one can see from the first line of Eq. (20), the system Eq. (19) contains a small parameter $\hbar$ and it is possible to use the standard scheme for solving asymptotically systems of linear differential equations [31], which represents the base of the WKB method. Notice that in matrix M, the energy $\mathcal{E}$ and total angular momentum J are the conserved quantities.

Following Ref. [31], one writes

$$\xi(r) = \varphi(r) \exp\left[\frac{i}{\hbar} S(r)\right], \tag{21}$$

which gives

$$\varphi'(r) = \frac{1}{\hbar}(M - iS' \cdot \sigma_0)\varphi(r), \quad S(r) = \int^r p(r)dr. \tag{22}$$

Then one seeks the solution of system Eq. (19) as an asymptotic series in powers of $\hbar$ (see, e.g., Ref. [32]):

$$p(r) = \sum_{n=0}^{\infty} \hbar^n p_n(r), \quad \varphi(r) = \sum_{n=0}^{\infty} \hbar^n \varphi^{(n)}(r). \tag{23}$$

Substituting these expansions in Eqs. (22) and equating the coefficients of equal powers of $\hbar$ to zero, we obtain an infinite system of recursive equations for the unknown scalar $p_n(r)$ and vector $\phi^{(n)}(r)$ functions,

$$(M - ip_0 I)\varphi^{(0)}(r) = 0, \tag{24a}$$

$$(M - ip_0 I)\varphi^{(n+1)}(r) = \varphi^{(n)'}(r) + i\sum_{l=0}^{n} p_{n+1-l}\varphi^{(l)}(r), \tag{24b}$$

where $l = 0, 1, \ldots n$. It follows from Eq. (24a) that ip_0 and $\varphi^{(0)}(r)$ must be the eigenvalues and eigenvectors of the matrix M. In particular, we find that $p_0(r) = \pm p(r)$ with

$$p(r) = \frac{\hbar}{l}\sqrt{\epsilon^2 - \delta^2 - j - \left(\frac{1}{4} - \beta^2\right)\rho^2 - \frac{j^2}{\rho^2} - 2\beta\epsilon\rho}. \tag{25}$$

Recall that $\rho = r/l$.

The WKB approximation for the 2D massless Dirac fermions was discussed in detail in Ref. [26], so we directly proceed to the analysis of our problem. In particular, the Bohr-Sommerfeld quantization condition for eigenenergies for the Dirac fermions was obtained in Ref. [26] both by using Zwaan's method and by considering the condition of single valuedness of the WKB wave function (see also Refs. [33,34]). It reads

$$I(\epsilon, j) \equiv \int_b^a dr p(r) = \pi\hbar\left(n_{\rm BS} + \frac{1 - \theta(-j)}{2}\right), \tag{26}$$

where $a \geqslant b$ are positive turning points [roots of the equation $p^2(r) = 0$], $n_{\rm BS} = 0, 1, 2, \ldots$ is the Bohr-Sommerfeld quantum number, $\theta(-j)$ is the step function [22] whose presence takes into account the spinor nature of the Dirac quasiparticles and the existence of the lowest $n = 0$ Landau level when the classically allowed region shrinks to a point.

A. WKB approximation in the absence of electric field

Let us recapitulate how the WKB method can be applied in the absence of an electric field, $E = 0$. In this case, the integral $I(\epsilon, j)$ on the left hand side (LHS) of the Bohr-Sommerfeld quantization condition Eq. (26) can be calculated:

$$I(\epsilon, j) = \frac{\hbar\pi}{2}(\epsilon^2 - \delta^2 - |j| - j). \tag{27}$$

Solving Eq. (26) for the energy ϵ, one recovers the well-known Landau-level spectrum,

$$\mathcal{E} = \pm\sqrt{\Delta^2 + (2n_{\rm BS} + j + |j| + 1 - \theta(-j))eH\hbar v_F^2/c}, \tag{28}$$

with $n_{\rm BS} = 0, 1, 2, \ldots$. Except for the asymmetric lowest Landau level, this result agrees perfectly with the exact solution of the Dirac equation in the symmetric gauge (see Appendix D of Ref. [35], where the final result is written in the form identical to the spectrum obtained in the Landau gauge). For $j < 0$, the spectrum Eq. (28) is consistent with the result in the Landau gauge if one identifies the quantum number $n_{\rm BS}$ and the Landau-level index $n = n_{\rm BS}$. To reproduce the spectrum for the $j > 0$ case, one should relabel the quantum numbers $2n = 2n_{\rm BS} + 2j + 1$, so n corresponds to the Landau-level index and $\mathcal{E} = \pm\sqrt{\Delta^2 + 2neH\hbar v_F^2/c}$ with $n = 1, 2, \ldots$ and $1/2 \leqslant j \leqslant n - 1/2$. Thus, one observes that in the absence of an electric field, the WKB method reproduces well-known exact results (see, for example, Ref. [26]).

B. WKB approximation in the radial electric field

Here we restrict ourselves to the gapless case, $\Delta = 0$. Then the expression Eq. (25) acquires the form

$$p(r) = \frac{\hbar\sqrt{1/4 - \beta^2}}{l\rho}\sqrt{-(\rho - \rho_1)(\rho - \rho_2)(\rho - \rho_3)(\rho - \rho_4)}, \tag{29}$$

where ρ_i are the roots of the quartic equation $p^2(r) = 0$:

$$\rho_{1,2} = \frac{-\epsilon \mp \sqrt{\epsilon^2 - 2j(1 - 2\beta)}}{1 - 2\beta},$$
$$\rho_{3,4} = \frac{\epsilon \mp \sqrt{\epsilon^2 - 2j(1 + 2\beta)}}{1 + 2\beta}. \tag{30}$$

As one can see, there are always two positive and two negative roots. In particular, for the zero electric case considered in Secs. III A and III C, the roots $\rho_1 = -\rho_4$ and $\rho_2 = -\rho_3$. This symmetry allows one to calculate the integral Eq. (27)

using the contour integration in the complex plane (see the corresponding integral in the textbook [36]).

Depending on the signs of ϵ and j, these roots are ordered as follows: for $\epsilon > 0$,

$$\begin{aligned} &\rho_1 < \rho_2 < 0 < \rho_3 < \rho_4 \quad \text{for} \quad j > 0, \\ &\rho_1 < \rho_3 < 0 < \rho_2 < \rho_4 \quad \text{for} \quad j < 0 \end{aligned} \tag{31}$$

and, for $\epsilon < 0$,

$$\begin{aligned} &\rho_3 < \rho_4 < 0 < \rho_1 < \rho_2 \quad \text{for} \quad j > 0, \\ &\rho_3 < \rho_2 < 0 < \rho_4 < \rho_2 \quad \text{for} \quad j < 0. \end{aligned} \tag{32}$$

For $\beta \to \mp 1/2$ and $\epsilon \gtrless 0$, the turning point ρ_4 (ρ_2) moves to infinity and some of the closed classical orbits transform into open trajectories.

We relabel these roots a, b, c, and d and assume that they obey the inequality $a > \rho > b > c > d$. Then the corresponding integral on the LHS of Eq. (26) can be expressed in terms of complete Legendre elliptic integrals of the first, $K(k)$, second, $E(k)$, and third $\Pi(\nu, k)$, kinds. In Appendix A, we obtain the following result:

$$I(\epsilon, j) = -\frac{\hbar}{\sqrt{1-4\beta^2}}[\beta\epsilon J_2 - (\epsilon^2 - j)J_1 + 2j^2 J_{-1}], \tag{33}$$

where

$$J_1 = \frac{2}{\sqrt{(a-c)(b-d)}}\left[(b-c)\Pi\left(\frac{a-b}{a-c}, k\right) + cK(k)\right], \tag{34a}$$

$$J_{-1} = \frac{2}{\sqrt{(a-c)(b-d)}}\left[\frac{c-b}{bc}\Pi\left(\frac{c(a-b)}{b(a-c)}, k\right) + \frac{1}{c}K(k)\right], \tag{34b}$$

$$\begin{aligned} J_2 = \frac{1}{\sqrt{(a-c)(b-d)}}\Big[&(-a(b-c) + c(b+c))K(k) \\ &+ (a-c)(b-d)E(k) \\ &+ (b-c)(a+b+c+d)\Pi\left(\frac{a-b}{a-c}, k\right)\Big], \end{aligned} \tag{34c}$$

with

$$k^2 = \frac{(a-b)(c-d)}{(a-c)(b-d)}. \tag{35}$$

The quantization condition Eq. (26) with the LHS given by Eq. (33) represents a transcendental equation for energies of bound states in terms of complete elliptic integrals. This complicated equation cannot be solved explicitly for the energy. However, they can be calculated efficiently with numerical methods. It is shown in Appendix C that the spectrum in the zero electric field, $E = 0$, limit can be directly derived from Eq. (33).

IV. RESULTS

A. The gapless case, $\Delta = 0$

To develop a qualitative understanding, it is useful to represent the momentum Eq. (25),

$$p(r) = \frac{\hbar}{l}\sqrt{\epsilon_{\text{eff}} - U_{\text{eff}}}, \tag{36}$$

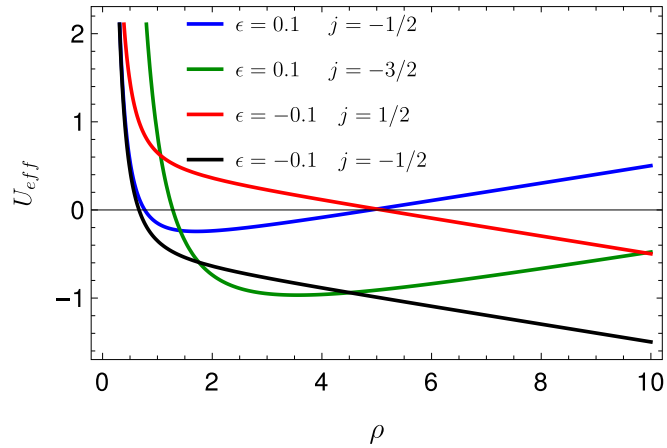

FIG. 2. The effective potential $U_{\text{eff}}(\rho)$ versus ρ for $\beta = 1/2$ and different values of ϵ and j.

in terms of the effective WKB energy $\epsilon_{\text{eff}} \equiv \epsilon^2$ (we set $\delta = 0$) and the effective potential:

$$U_{\text{eff}}(\rho) \equiv \left(\frac{1}{4} - \beta^2\right)\rho^2 + 2\beta\epsilon\rho + \frac{j^2}{\rho^2} + j. \tag{37}$$

It is clear from Eqs. (29)–(32) that the classically allowed region is situated between the positive roots denoted above as $a > \rho > b > 0$. One can see that a finite motion and quantized energy levels are possible for $|\beta| < 1/2$ when the potential Eq. (37) grows as $\rho \to \infty$. Furthermore, for $\beta = \pm 1/2$ the character of motion becomes dependent on the linear in ρ and constant terms of the potential Eq. (37) (see Fig. 2). We return to this point below.

For comparison, we recapitulate that for the problem with the repulsive Coulomb potential $V(r) = \hbar v_F \mathfrak{g}/r$ with dimensionless coupling $\mathfrak{g}$ [26] (see also Refs. [24,25,28]), the effective potential

$$U^C_{\text{eff}}(\rho) \equiv \frac{\rho^2}{4} + \frac{2\mathfrak{g}\epsilon}{\rho} + \frac{j^2 - \mathfrak{g}^2}{\rho^2} + j. \tag{38}$$

In contrast to the case considered in this paper, the effective potential for the Coulomb interaction is always positive as $\rho \to \infty$ and the behavior of the system is determined by its dependence for $\rho \to 0$. The critical value of $\mathfrak{g}$ when $U^C_{\text{eff}}(\rho)$ becomes negative turns out to be dependent on the absolute value of total angular momentum quantum number j.

1. Numerical solution in WKB approximation

The Bohr-Sommerfeld quantization condition Eq. (26) with the LHS given by Eq. (33) represents the transcendental WKB equation for the energy spectrum. Its numerical solution describing the dependence of the energy $\mathcal{E}$ in units $\epsilon_0 = \hbar v_F/l$ versus electric field in terms of the dimensionless parameter β is shown in Fig. 3. For better readability, we plotted the cases $j > 0$ and $j < 0$ on the separate left (a) and right (b) panels, respectively.

For $j > 0$, we have done the relabeling of the Landau levels as described below Eq. (28), so the notation $n = 1, 2, 3, 4$ corresponds to the Landau-level index. The lowest $n = 0$ level is present only for $j < 0$.

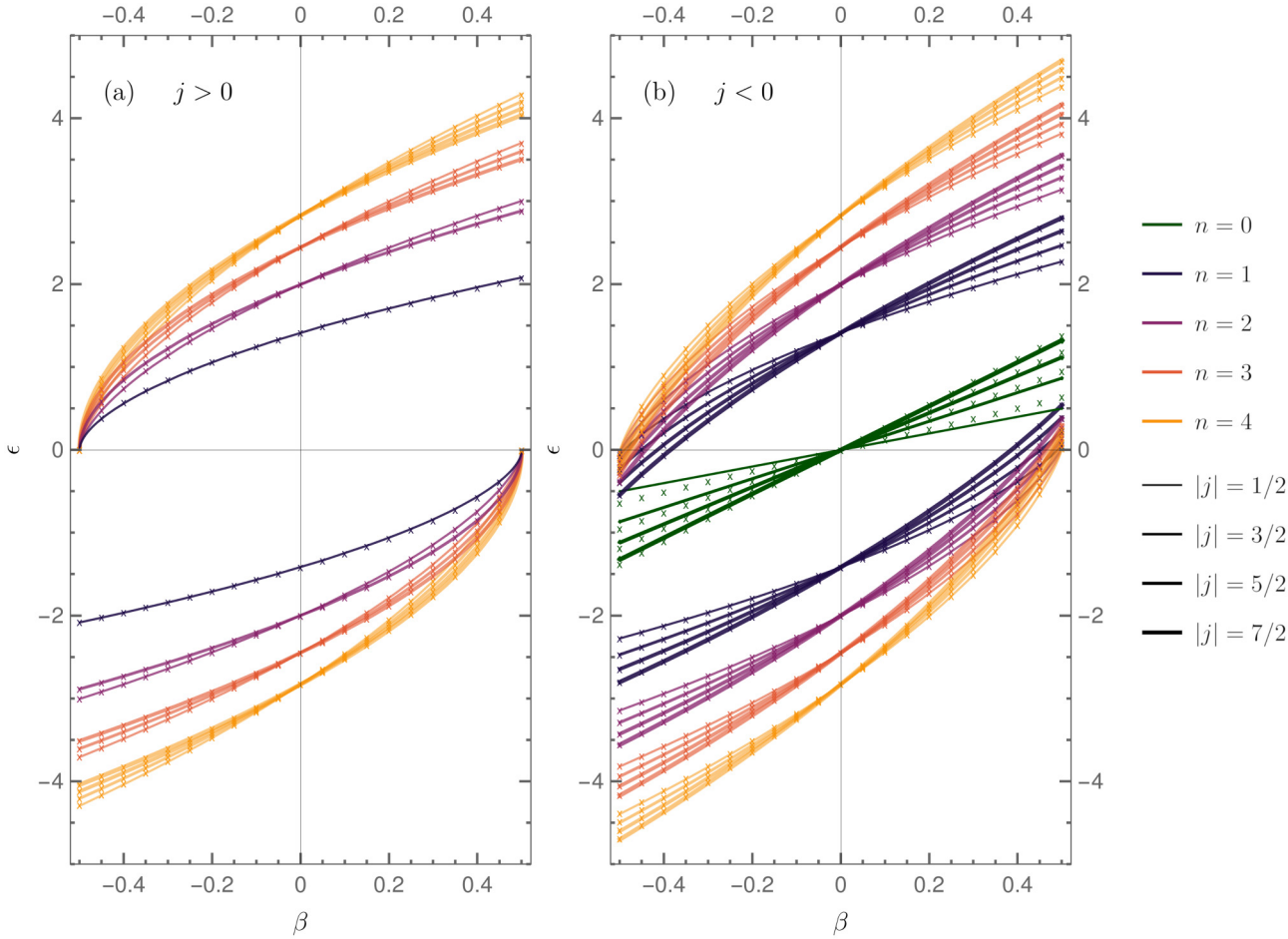

FIG. 3. WKB and exact diagonalization (ED) spectra in units $\epsilon_0 = \hbar v_F/l$ versus electric field in terms of $\beta = cE/(v_F H)$ for the gapless $\Delta = 0$ case. Panel (a) shows positive values of j and panel (b) shows negative values of j. In both panels, solid lines show the results of the WKB approximation and crosses show the results calculated using ED. The Landau levels with $n = 0, 1, 2, 3, 4$ are shown by the green, dark purple, purple lines, red and orange lines, respectively. The levels with $|j| = 1/2, 3/2, 5/2, 7/2$ are marked by the increasing thickness of the lines.

First, we observe that the presence of a finite electric field removes the degeneracy of the Landau levels with the different total angular momenta $|j| = 1/2, 3/2, 5/2, 7/2$ that are marked by the increasing thickness of the lines, respectively. As discussed below Eq. (28), for $j > 0$ to keep n being the Landau-level index, one should set a restriction on the allowed values of the total angular momentum quantum number $1/2 \leqslant j \leqslant n - 1/2$. Thus, for $n = 1$ there is only one line with $j = 1/2$; for $n = 2$ there are two lines with $j = 1/2, 3/2$ and so on. On the other hand, there is no such restriction for the negative values of j and we just restricted ourselves by showing the lines with $j = -1/2, -3/2, -5/2, -7/2$. The apparent asymmetry in the allowed range of the values of j reflects that circulating with positive j in the presence of a magnetic field directed in the positive z direction costs energy for an electron, whereas circulating with negative j does not [37].

For $E = 0$, these levels become degenerate and their energies are in agreement with Eq. (28). One can see that the dependencies $\epsilon(\beta)$ for the electronlike levels are symmetric with respect to the coordinate origin, $\epsilon(\beta) = -\epsilon(-\beta)$, as compared to the corresponding dependencies $\epsilon(\beta)$ for the holelike levels in both panels [see Eq. (38)].

An interesting property of the presented results is that the character of the dependence of the spectra on β turns out to depend on the sign of j. The holelike Landau levels with different values of $j > 0$ and given n are nondegenerate for $\beta = -1/2$. Then, as β increases the distance between these levels diminishes and they become degenerate as β reaches zero. Then, as β becomes positive, the distance between the levels starts to increase, but when β grows further the distance between the levels diminishes and all levels with different $j > 0$ and $n \geqslant 1$ collapse to zero energy for $\beta = 1/2$. The behavior of the electronlike levels is consistent with above-mentioned symmetry, so their collapse occurs as β decreases from $1/2$ to $-1/2$.

This critical value $\beta = 1/2$ first appears in Ref. [27], where Coulomb impurity spectra under external electric and magnetic fields were studied using the coupled series expansion method. Although the main focus of Ref. [27] is on the Coulomb impurity, it also contains some numerical results corresponding to the field configuration considered here.

The behavior of levels with $j < 0$ is drastically different. First, these levels include the $n = 0$ Landau level whose energy depends linearly on the electric field. The holelike levels for $-1/2 \leqslant \beta \leqslant 0$ behave similarly to the positive j case. However, for $0 \leqslant \beta \leqslant 1/2$ the level distances increase and as β gets closer to $1/2$ the levels with $j = -7/2, -5/2, -3/2, -1/2$ one by one cross zero and have positive constant values at $\beta = 1/2$. There is no level collapse in this case. The behavior of the electronlike levels is consistent with the above-mentioned symmetry, so the level distances increase and their energies become negative as β decreases from $1/2$ to $-1/2$.

The values of β for which the negative-j levels intersect the zero energy line can be found analytically. Indeed, the function $I(\epsilon = 0, j)$ defined by Eq. (26) acquires a rather simple form,

$$I(\epsilon = 0, j) = \hbar \int_{\rho_1}^{\rho_2} d\rho \sqrt{-(1/4 - \beta^2)\rho^2 - \frac{j^2}{\rho^2} - j}, \quad (39)$$

with $\rho_\pm = \sqrt{(-2j)/(1 \pm 2|\beta|)}$. Evaluating the integral Eq. (39) and substituting the result in Eq. (26), we arrive at the equation that determines the intersection points $\beta = \beta(\epsilon = 0, n, j)$, which can be solved explicitly:

$$\beta(n, j) = \pm \frac{\sqrt{n(n + |j|)}}{2n + |j|}, \quad j < 0, \ n = 0, 1, \ldots. \quad (40)$$

Here we took into account that $n = n_{\mathrm{BS}}$ for $j < 0$. Since the nontrivial solutions Eqs. (40) exist for all allowed values of n and $j < 0$, this proves that all corresponding levels cross zero energy.

As mentioned above, the levels $\epsilon(n, j, \beta)$ approach the bound-state energies $\epsilon(n, j, \beta = 1/2)$ as β reaches the value $1/2$. We have also obtained Eq. (B6) (see Appendix B) for these energies $\epsilon(n, j, \beta = 1/2)$ and found its approximate analytic solution:

$$\epsilon(n, j, \beta = 1/2) \approx \left(\frac{|j|}{2} - \sqrt{\frac{3\sqrt{3} n |j|}{2}} \right)^{1/2}, \quad |j| \gg \pi n. \quad (41)$$

The numerical solution of Eq. (B6) for the eigenenergies $\epsilon(n, j, \beta = 1/2)$ versus the total angular momentum quantum number j is shown in Fig. 4 by the large blue dots. The approximate solution Eqs. (41) is plotted for comparison (small green dots). One can see that the approximate solution has a good agreement with the numerical one for large values of j.

As follows from Figs. 3, 4, and analytic consideration, for $\beta = 1/2$ there are bound states for positive energies, ϵ, irrespective to the sign of j, and bound states are absent for negative energies, ϵ. To explain this, we plotted in Fig. 2 the effective potential Eq. (37) for $\beta = 1/2$ and different values of ϵ and j.

As mentioned above for $\beta = 1/2$, the behavior of the potential is governed by the last three terms of Eq. (37). For $\epsilon > 0$, the effective potential $U_{\mathrm{eff}}(\rho)$ grows linearly as $\rho \to \infty$, so the quasiparticle orbits remain closed and correspond to the bound states. For $\epsilon < 0$, the effective potential $U_{\mathrm{eff}}(\rho)$ decreases linearly as $\rho \to \infty$, so there are no closed orbits and bound states. Since for $j < 0$ the solutions for $\beta = 1/2$ have the positive energy and thus are the bound states, there is no Landau-level collapse in this case.

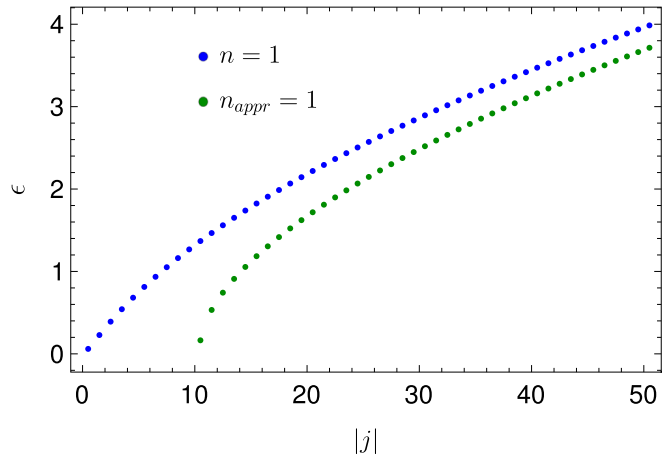

FIG. 4. The WKB eigenenergies $\epsilon(n, j, \beta = 1/2)$ versus the total angular momentum quantum number j for $n = 1$. Large blue dots correspond to the numerical solution of Eq. (B6) and small green dots are for the approximate solution Eqs. (41).

On the other hand, for $j > 0$ all levels with negative energy merge to one point and collapse (see Fig. 3 left panel). It is important to stress that because for $j > 0$ the expression under the square root in the integrand of Eq. (39) is negative, Eq. (26) does not have a solution in this case. Thus, in contrast to the case of the crossed uniform magnetic and electric fields, in the studied geometry the collapse points with $\epsilon = 0$ and $\beta = \pm 1/2$ do not belong to the spectra.

2. Diagonalization and shooting method

To verify the accuracy of the WKB approximation, we use two numerical methods: discretization with exact diagonalization and shooting method.

For the diagonalization method, we use the Hamiltonian which one can obtain from Eq. (20). To do this, one should rewrite Eq. (20) in terms of an eigenvalue problem multiplying it by $i\sigma_2$ matrix. The first derivative (momentum) is discretized using finite differences. In this way, the eigenvalue problem can be solved on a 1D lattice with two orbitals, where the momentum is turned into hopping terms and the other parts of the Hamiltonian into on-site terms.

It is worth noting that the choice of grid spacing of the lattice should correspond to the behavior of the on-site term to reach all important values. To increase the efficiency, we use a nonconstant grid with slowly increasing spacing, thus obtaining more dots closer to zero, where our effective potential is singular.

To implement the discretization method, the KWANT [38] Python package was used. With this package, we build the Hamiltonian of a 2000-site-long chain and then numerically diagonalize it.

It also should be noted that with such a method one can obtain a fermionic-doubling effect [39], as we observe in our numerical work. Although this effect is not clearly seen in the gapless case, it immediately appears if one introduces a nonzero gap, thus resulting in the spectra doubling.

The shooting method is an integration process performed on the system Eq. (20) with a guessed energy-parameter (for more details, see Appendix D). Such a method does not result in the fermionic doubling. Thus we can numerically solve the corresponding equations for each $\mathbf{K}_\pm$ separately and prove that the diagonalization method produces the results for the two valleys together.

The exact diagonalization method is more efficient in a sense of speed and precision in comparison with shooting. Thus, we use the diagonalization as a main computation method and the shooting method as an auxiliary one to distinguish different $\mathbf{K}_\pm$ valleys.

The results of the numerical methods described above for the gapless case are shown in Fig. 3 by crosses. The comparison with WKB (solid lines in Fig. 3) shows that the WKB approximation is in a good quantitative agreement with the numerical calculations for the whole range of the values of β, j, and n. There are only small quantitative discrepancies in the energies of the lowest, $n = 0$, Landau level seen in Fig. 3(b). However, this deviation decreases with increasing $|j|$. The gapped case was investigated using numerical methods only and is considered in what follows.

B. The gapped case

Now we turn to the finite Δ case. A crucial feature is that the fully quantum mechanical description of the problem, as one can see from the second-order Eq. (18) [see also Eqs. (11) and (12)] is sensitive to the sign of Δ when β is nonzero. As mentioned above Eq. (9), the solution at the $\mathbf{K}_-$ point is obtained from the solution at the $\mathbf{K}_+$ point by changing $\Delta \to -\Delta$. Thus, for finite values of gap Δ and electric field E, the results for the spectra are expected to be valley dependent.

On the other hand, one can see from Eq. (25) that even for a finite δ the WKB approximation does not distinguish the valley because it contains only δ^2.

The fully numerical solution obtained using the methods described in Sec. IV A 2 for the dependence of the energy $\mathcal{E}$ in units $\epsilon_0 = \hbar v_F/l$ versus electric field in terms of the dimensionless parameter β in the finite δ case is shown in Fig. 5. We used the same color and thickness scheme as the one displayed in Fig. 3, but for clarity of the figure we do not include the $n = 4$ level and $|j| = 7/2$ (see also Supplemental Material [40]).

Similarly to Fig. 3, cases $j > 0$ and $j < 0$ are shown on the separate (a) and (b) panels, respectively. However, in Fig. 5(a), we selected a larger value of $\delta = 3$ to make more distinct the difference between the gapped (solid lines) and gapless (dashed lines) cases. In both cases, the levels with different $j > 0$ and $n \geqslant 1$ collapse to zero energy for $|\beta| = 1/2$.

One can see that in the contrast to the gapless case (see Fig. 3), the dependencies $\epsilon(\beta)$ for the energy levels levels are no more symmetric with respect to the coordinate origin.

Yet, in the absence of an electric field the positive and negative energy levels are symmetric with respect to the zero energy except for the lowest $n = 0$ Landau level [35]. Since as discussed below Eq. (28) for $j > 0$, the Landau-level index takes the values $n = 1, 2, \ldots$, the lowest level is absent in Fig. 5(a), so for $\beta = 0$ all electron- and holelike levels are symmetric with respect to the origin. The lowest Landau level is present in Figs. 3(b) and 5(b). Notice that for the chosen $\mathbf{K}_+$ point and direction of the magnetic field, the energy of this level has to be $-\Delta$ for $E = 0$ [35]. This agrees with Fig. 5(b), where the Landau levels for only the $\mathbf{K}_+$ point are shown. [Recall that Fig. 5(a) also contains the Landau levels for the $\mathbf{K}_+$ point and there is no difference between the $\mathbf{K}_\pm$ points in the gapless case considered in Sec. IV A.]

This asymmetry of the energy of the lowest Landau level for $\beta = 0$ would disappear if one takes into consideration the second $\mathbf{K}_-$ point with the lowest level having a positive energy Δ for $E = 0$. Note that the general asymmetry between the electron- and holelike levels with respect to the coordinate origin for $\delta, \beta \neq 0$ would also disappear when the levels for $\mathbf{K}_-$ point are considered. It is worth mentioning that as follows from Eq. (3) this valley asymmetry is absent in the crossed uniform magnetic and electric fields configuration.

To obtain Fig. 5(b), we took a smaller value of the gap $\delta = \sqrt{2}$ such that $|j| < \delta^2$ for $j = -1/2, -3/2$ and $|j| > \delta^2$ for $j = -5/2$. To resolve the $\epsilon(\beta)$ dependencies in the vicinity of $\beta = 1/2$, a zoom of this region is shown in Fig. 5(c). One can see that the levels with $j = -1/2, -3/2$ collapse to zero energy, while the levels with $j = -5/2$ cross zero and approach positive constant values. The evolution of Landau levels with the increase of the gap is presented in the Supplemental Material [40].

Generalizing the analysis of Eq. (39) for the finite δ case, one finds that the energy levels may cross the $\epsilon = 0$ line if $|j| > \delta^2$. The levels with $|j| < \delta^2$ cannot cross this line and thus approach the $\epsilon = 0$ point for $|\beta| = 1/2$.

This behavior may also be understood qualitatively by considering Fig. 2 for the effective potential plotted for various values of j. The classically allowed region is determined by the points where $U_{\text{eff}}(\rho)$ crosses the effective energy $\epsilon_{\text{eff}} = \epsilon^2 - \delta^2$. For $\delta = 0$ and $\beta = 1/2$, the positive-j levels collapse and the negative-j levels correspond to the bound states with $\epsilon > 0$. However, the presence of a finite δ shifts down the values of $j < 0$ allowed for the collapse by $-\delta^2$.

Thus, the presence of the gap extends the values of j allowed for the Landau level collapse from positive-j to the negative-j levels with $|j| < \delta^2$.

V. CONCLUSION

As already mentioned in the Introduction, the Landau-level collapse was already observed experimentally [8,9]. For example, in Ref. [9] the Shubnikov–de Haas-type resonances arising from quantized states associated with closed orbits are used to directly observe the competition between magnetic confinement and deconfinement due to electric field. While these observations were made in the rectangular geometry, there are no limitations for repeating them in the circular Corbino geometry considered in this work.

High-mobility Corbino devices in a dual-gated geometry were recently studied in Ref. [41]. Bulk conductance measurement outperforms previously reported Hall bar measurements and allowed one to observe both the integer and fractional QHE states. It should be technically possible to modify the existing devices introducing the radial electric field by gating. Another way to apply the radial electric field might be achieved by injecting a high-current density in the device [8].

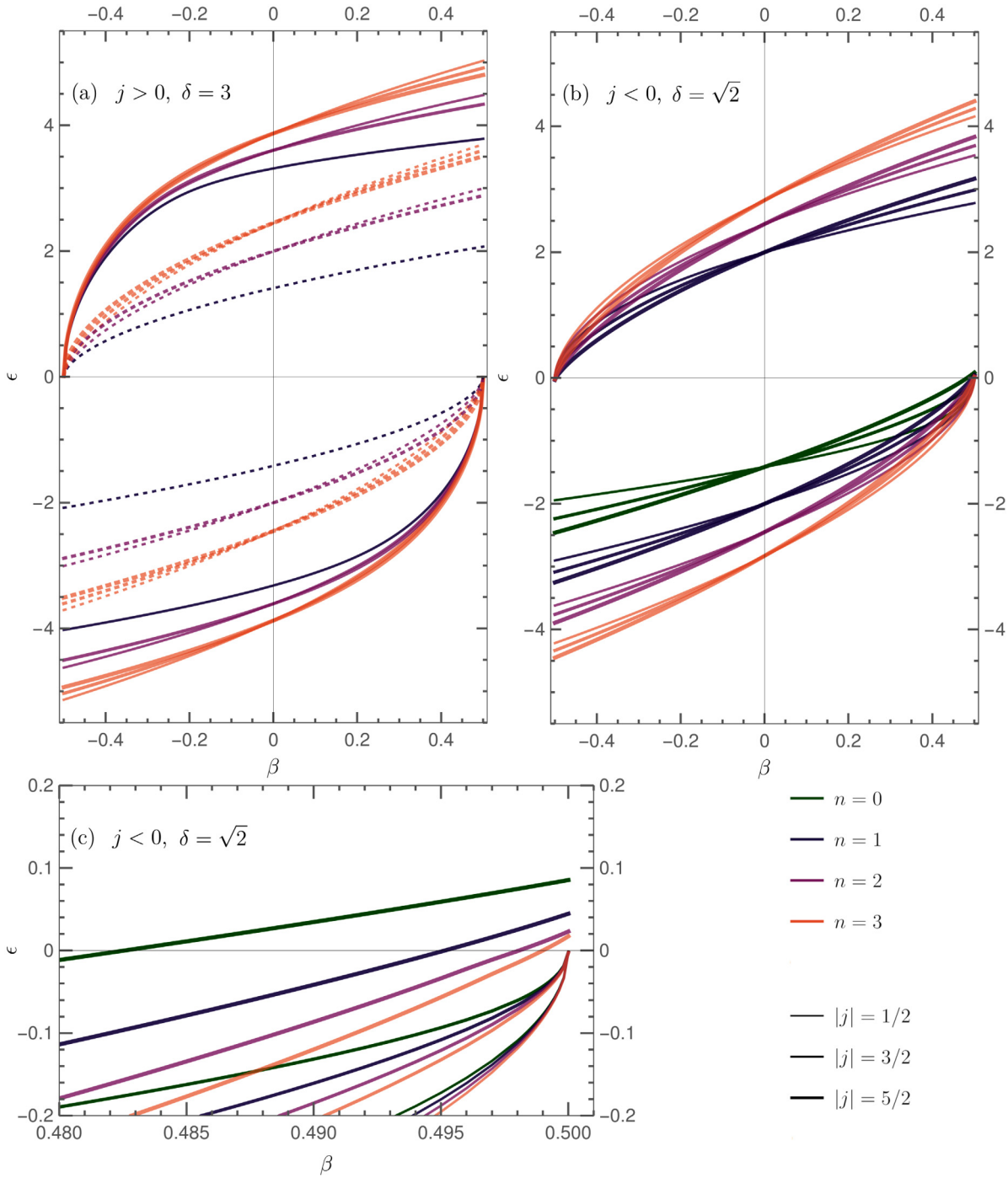

FIG. 5. Spectra for the $\mathbf{K}_+$ point obtained by the shooting method in units $\epsilon_0 = \hbar v_F/l$ versus electric field in terms of $\beta = cE/(v_F H)$ for the finite gap, $\delta = l\Delta/(\hbar v_F)$, case. (a) Positive j: The solid lines are the solutions for $\delta = 3$ and the dashed lines are for $\delta = 0$. (b) Negative j: The gap $\delta = \sqrt{2}$. (c) The zoom of plot (b) in the vicinity of $\beta = 1/2$. The same color and thickness scheme as the one displayed in Fig. 3 is used.

Since for nonzero electric field the degeneracy of the Landau levels with different total angular momenta j is lifted, this should be manifested in the transport measurements. Another possibility to observe the predicted features is to employ scanning tunneling spectroscopy that allowed one to observe Dirac Landau levels in graphene [42].

Further increase of the electric field would allow one to realize the Landau-level collapse in the geometry studied in this paper. Moreover, the critical electric field required for the collapse is $\pm E_c/2$ is twice smaller than the corresponding field $E_c = (v_F/c)H$ for the rectangular geometry that should make its observation easier. In contrast to the rectangular geometry, the collapse in the circular geometry is sensitive to the sign of the electric filed, so the hole (electron)-like levels collapse at $+(-)E_c/2$. One can estimate that for the magnetic field $H = 1\,\mathrm{T}$ and the Fermi velocity $v_F = 1 \times 10^6\,\mathrm{m/s}$, the

critical electric field in the circular geometry is $E_c = 0.5 \times 10^4$ V/cm which should be possible to create by gating.

It should also be possible to investigate the collapse in the gapped case by using graphene placed on top of hexagonal boron nitride (G/hBN).

Another experimental setup that would allow one to realize the Landau-level collapse by generating strain induced either pseudomagnetic or electric fields was suggested in Refs. [43,44], respectively. Although the corresponding experiments were not done, it should be possible to make them both in rectangular and Corbino geometries. Finally, it might also be necessary to generalize the presented results with a radial electric field for a finite-size Corbino disk [45].

ACKNOWLEDGMENTS

I.O.N. and V.K. would like to thank I.C. Fulga and J. van den Brink for fruitful discussions. I.O.N., V.P.G., and S.G.Sh. are grateful to O.O. Sobol for valuable discussions. V.P.G. and S.G.Sh. thank A.A. Varlamov for useful remarks. I.O.N., V.P.G., and S.G.Sh. acknowledge support by the National Research Foundation of Ukraine (NRFU) Grant No. 2020.02/0051, Topological Phases of Matter and Excitations in Dirac Materials, Josephson Junctions and Magnets.

APPENDIX A: CALCULATION OF THE INTEGRAL $I(\epsilon, j)$ FOR FINITE β

We calculate the integral Eq. (33),

$$I(\epsilon, j) = \sqrt{1/4 - \beta^2} S, \tag{A1}$$

with

$$S = \int_b^a \frac{dx\, y(x)}{x}, \tag{A2}$$

and $y(x) = \sqrt{(a-x)(x-b)(x-c)(x-d)}$. Here we introduced notations of Ref. [46], where similar integrals are calculated. Multiplying the numerator and denominator of the integrand in Eq. (A2) by $y(x)$, one obtains

$$S = \int_b^a \frac{a_0 x^3 + 4a_1 x^2 + 6a_2 x + 4a_3 + a_4/x}{y(x)}, \tag{A3}$$

where $y^2(x) = a_0 x^4 + 4a_1 x^3 + 6a_2 x^2 + 4a_3 x + a_4$ with

$$\begin{aligned} &a_0 = -1, \quad 4a_1 = a + b + c + d, \\ &6a_2 = -a(b+c) - b(c+d) - d(a+c), \\ &4a_3 = acd + bcd + abc + abd, \quad a_4 = -abcd. \end{aligned} \tag{A4}$$

Accordingly, for the relabeled roots $\rho_4 \to a$, $\rho_3 \to b$, $\rho_2 \to c$, $\rho_1 \to d$ (recall that we assumed that $a > x > b > c > d$), one obtains that

$$\begin{aligned} &a_0 = -1, \quad a_1 = -\frac{2\beta\epsilon}{1-4\beta^2}, \quad a_2 = \frac{2(\epsilon^2 - j)}{3(1-4\beta^2)}, \\ &a_3 = 0, \quad a_4 = -\frac{4j^2}{1-4\beta^2}. \end{aligned} \tag{A5}$$

Defining the integrals

$$J_n = \int_b^a \frac{dx\, x^n}{y(x)}, \quad n = -1, 0, 1, 2, 3, \tag{A6}$$

one can rewrite Eq. (A3) in the following form:

$$S = a_0 J_3 + 4a_1 J_2 + 6a_2 J_1 + 4a_3 J_0 + a_4 J_{-1}. \tag{A7}$$

To get rid of the integral J_3 from Eq. (A7), we consider the derivative

$$\frac{dy}{dx} = \frac{2a_0 x^3 + 6a_1 x^2 + 6a_2 x + 2a_3}{y}, \tag{A8}$$

and integrating it b to a we obtain the identity

$$a_0 J_3 + 3a_1 J_2 + 3a_2 J_1 + a_3 J_0 = 0. \tag{A9}$$

Hence

$$S = a_1 J_2 + 3a_2 J_1 + 3a_3 J_0 + a_4 J_{-1}, \tag{A10}$$

and using the coefficients Eqs. (A5) we arrive at the expression

$$S = -\frac{2}{1-4\beta^2}[\beta\epsilon J_2 - (\epsilon^2 - j)J_1 + 2j^2 J_{-1}]. \tag{A11}$$

The integrals J_1 and J_{-1} given by Eqs. (34a) and (34b), respectively, can be found in Ref. [47] [see Eqs. (3.148.6) and (3.150.4)]. The integral J_2 is considered, for example, in Ref. [48], where it is rewritten in the form

$$\begin{aligned} J_2 = \frac{2}{\sqrt{(a-c)(b-d)}}\Bigg[&c^2 K(k) + 2c(b-c) \\ &\times \Pi\left(\frac{a-b}{a-c}, k\right) + (b-c)^2 T_2\left(\frac{a-b}{a-c}, k\right)\Bigg], \end{aligned} \tag{A12}$$

where

$$T_2(\nu, k) = \int_0^{\pi/2} \frac{d\varphi}{(1 - \nu \sin^2\varphi)^2 \sqrt{1 - k^2 \sin^2\varphi}}. \tag{A13}$$

Evaluating the last integral (see Eq. (2.592.6) in Ref. [47]), one obtains

$$\begin{aligned} T_2(\nu, k) = &-\frac{1}{2(1-\nu)} K(k) - \frac{\nu}{2(k^2 - \nu)(1-\nu)} E(k) \\ &+ \frac{k^2(3-2\nu) + \nu(\nu-2)}{2(k^2-\nu)(1-\nu)} \Pi(\nu, k). \end{aligned} \tag{A14}$$

Finally, substituting (A14) in Eq. (A12), we obtain Eq. (34c).

APPENDIX B: CALCULATION OF THE INTEGRAL $I(\epsilon, j, \beta = 1/2)$ AND ENERGIES $\epsilon(n, j, \beta = 1/2)$

We provide below the results of the analytical consideration of the $\beta = 1/2$ case. Formally, an equation for the energies $\epsilon(n, j, \beta = 1/2)$ is still given by the Bohr-Sommerfeld quantization condition Eq. (26), but its LHS is simpler than the generic expression in Eq. (33). Indeed, the expression for the momentum Eq. (25) acquires a more simple form than Eq. (29),

$$p(r) = \frac{\hbar}{l\rho}\sqrt{-\epsilon(\rho - \rho_1)(\rho - \rho_2)(\rho - \rho_3)}, \tag{B1}$$

where the roots of the cubic equation $p^2(r) = 0$ are

$$\rho_{1,2} = \frac{\epsilon \pm \sqrt{\epsilon^2 - 4j}}{2}, \quad \rho_3 = -\frac{j}{\epsilon}. \tag{B2}$$

Again, depending on the signs of ϵ and j, these roots are ordered differently.

The calculation of $I(\epsilon, j, \beta = 1/2)$ is rather similar to the general case considered in Appendix A and we restrict ourselves by showing the final result. We obtain

$$I(\epsilon, j, \beta = 1/2) = \frac{\hbar}{\sqrt{\epsilon}}\left(\frac{\epsilon^2 - j}{3}L_1 - j^2 L_{-1}\right), \tag{B3}$$

where

$$L_n = \int_b^a \frac{dx x^n}{\sqrt{(a-x)(x-b)(x-c)}}, \quad a > b > c, \tag{B4}$$

with $n = -1, 1$. Using Eqs. (3.132.5) and (3.137.6) from Ref. [47], we have

$$L_1 = \frac{2c}{\sqrt{a-c}}K(k) + 2\sqrt{a-c}E(k), \tag{B5a}$$

$$L_{-1} = \frac{2}{a\sqrt{a-c}}\Pi\left(\frac{a-b}{a}, k\right), \tag{B5b}$$

with $k^2 = (a-b)/(a-c)$.

In the considered $\epsilon > 0$ and $j < 0$ case, we have $a = \rho_3 = |j|/\epsilon$, $b = \rho_1$ and $c = \rho_2$. Substituting Eq. (B3) in the quantization condition Eq. (26) we arrive at the following transcendental equation for the eigenenergy $\epsilon(j, n, \beta = 1/2)$:

$$\frac{\sqrt{2}}{3\sqrt{ts}}[(t+1)sE(k) + (t+1)(t - \sqrt{t^2+4t})K(k) - 6t\Pi(\nu, k)] = \frac{\pi n}{|j|}, \tag{B6}$$

where we introduced $t = \epsilon^2/|j|$ and

$$s = 2 - t + \sqrt{t^2+4t}, \quad r = 2 - t - \sqrt{t^2+4t},$$
$$\nu = 1 - \frac{t + \sqrt{t^2+4t}}{2}, \quad k^2 = \frac{r}{s}. \tag{B7}$$

In the limit $|j| \to \infty$, Eq. (B6) has an exact solution $t = 1/2$, so asymptotically $\epsilon \sim \sqrt{|j|/2}$. Expanding the LHS of Eq. (B6) around the point $t = 1/2$ up to $(t-1/2)^2$ term one obtains the following equation:

$$\frac{2\pi}{3\sqrt{3}}\left(t - \frac{1}{2}\right)^2 = \frac{\pi n}{|j|}, \tag{B8}$$

which leads to the expression Eq. (41) in the main text.

APPENDIX C: LIMIT $E = 0$ FROM EQ. (33)

Here we show that the Bohr-Sommerfeld quantization condition Eq. (26) with the LHS given by Eq. (33) in the absence of an electric field produces the spectrum Eq. (28) with $\Delta = 0$. For $\beta = 0$, the first term of Eq. (33) disappears,

$$I(\epsilon, j, \beta = 0) = \hbar[(\epsilon^2 - j)J_1 - 2j^2 J_{-1}], \tag{C1}$$

and as mentioned above Eq. (31), the arguments of J_{-1} and J_1 have opposite values $d = -a$ and $c = -b$. Then Eqs. (34a) and (34b) are simplified to the form

$$J_1 = \frac{2}{a+b}[2b\Pi(k, k) - bK(k)], \tag{C2a}$$

$$J_{-1} = \frac{2}{a+b}\left[\frac{2}{b}\Pi(-k, k) - \frac{1}{b}K(k)\right], \tag{C2b}$$

with $k = (a-b)/(a+b)$.

For definiteness, we choose the case $\epsilon > 0$, $j > 0$ corresponding to the first line of Eq. (31) that gives

$$a = \epsilon + \sqrt{\epsilon^2 - 2j}, \quad b = \epsilon - \sqrt{\epsilon^2 - 2j},$$
$$k = \frac{\sqrt{\epsilon^2 - 2j}}{\epsilon}. \tag{C3}$$

Rewriting the relation Eq. (19.6.2) from Ref. [49] as

$$\Pi(\pm k, k) = \frac{\pi}{4(1 \mp k)} + \frac{1}{2}K(k), \tag{C4}$$

one can verify that Eq. (C1) reduces to

$$I(\epsilon, j, \beta = 0) = \hbar\frac{\pi}{2}(\epsilon^2 - 2j), \tag{C5}$$

which agrees with Eq. (27) for $\delta = 0$ and $j > 0$. This completes the proof that one can recover the spectrum (28) with $\Delta = 0$ from the quantization condition Eq. (26) with the LHS given by Eq. (33) by setting $\beta = 0$.

APPENDIX D: SHOOTING METHOD

Equation (20) for the spinor components $f(\rho)$ and $g(\rho)$ defined by Eq. (10) has the form

$$\frac{df(\rho)}{d\rho} = \left(\frac{j}{\rho} + \frac{\rho}{2}\right)f(\rho) + (\beta\rho - \varepsilon - \delta)g(\rho),$$
$$-\frac{dg(\rho)}{d\rho} = \left(\frac{j}{\rho} + \frac{\rho}{2}\right)g(\rho) + (\beta\rho - \varepsilon + \delta)f(\rho). \tag{D1}$$

One can obtain from Eqs. (D1) the derivative df/dg. It can be integrated up to a constant which is taken to be equal to zero, because the subsequent equation should have a trivial solution $f = g = 0$ as $\rho \to \infty$:

$$f^2(\beta\rho - \varepsilon + \delta) + 2gf\left(\frac{j}{\rho} + \frac{\rho}{2}\right) + g^2(\beta\rho - \varepsilon - \delta) = 0. \tag{D2}$$

Thus, the ratio $f(\rho)/g(\rho)$ can be obtained. Using it, we can guess the initial value for one function and then calculate the initial value for the other one. The boundary values at $\rho \to \infty$ are expected to be zero, since functions $f(\rho)$, $g(\rho)$ have to be square integrable.

Now, when we know the initial and boundary conditions, we perform an integration process on the system Eq. (D1) setting the numeric value of ε from an interval of interest. Such a method is called a shooting method; for more details see Ref. [50]. To do the integration, we use the Runge-Kutta sixth-order method. The boundaries for integration are $\rho \in [0.001, 100]$, where the beginning of the interval replaces zero (which is a point of singularity in the system) and the end replaces the infinity (in this case, $r = l\rho$ is comparable to the length of the chain used in the diagonalization method).

Shooting with energies from an interval of interest and performing a numerical integration from some initial values, one can obtain a dependence of $f(\rho \to \infty)$ [or $g(\rho \to \infty)$] on the energy ε. Such a function goes through zero every time the energy value is guessed correctly. This allows us to use a bisection method on the mentioned dependencies to calculate the energies.

[1] I. Rabi, Z. Phys. **49**, 507 (1928).

[2] Y. I. Frenkel and M. P. Bronstein, J. Russian Phys. Chem. Soc. **62**, 485 (1930).

[3] L. D. Landau, Z. Phys. **64**, 629 (1930).

[4] K. S. Novoselov, A. K. Geim, S. V. Morozov, D. Jiang, M. I. Katsnelson, I. V. Grigorieva, S. V. Dubonos, and A. A. Firsov, Nature (London) **438**, 197 (2005).

[5] Y. Zhang, Y.-W. Tan, H. L. Stormer, and P. Kim, Nature (London) **438**, 201 (2005).

[6] V. Lukose, R. Shankar, and G. Baskaran, Phys. Rev. Lett. **98**, 116802 (2007).

[7] N. M. R. Peres and E. V. Castro, J. Phys.: Condens. Matter **19**, 406231 (2007).

[8] V. Singh and M. M. Deshmukh, Phys. Rev. B **80**, 081404(R) (2009).

[9] N. Gu, M. Rudner, A. Young, and P. Kim, and L. Levitov, Phys. Rev. Lett. **106**, 066601 (2011).

[10] I. M. Lifshitz and M. I. Kaganov, Usp. Fiz. Nauk **69**, 419 (1959) [Sov. Phys. Usp. **2**, 831 (1960)].

[11] I. M. Lifshitz, M. Y. Azbel, M. I. Kaganov, *Electron Theory of Metals* (Consultants Bureau, New York, 1973).

[12] Z. Z. Alisultanov, Phys. B: Condens. Matter **438**, 41 (2014).

[13] A. Shytov, M. Rudner, N. Gu, M. Katsnelson, and L. Levitov, Solid State Commun. **149**, 1087 (2009).

[14] V. Arjona, E. V. Castro, and M. A. H. Vozmediano, Phys. Rev. B **96**, 081110(R) (2017).

[15] Note that SI units are used, for example, in Ref. [14]. Accordingly, Lorenz transformations for the fields and other equations in SI units are recovered by replacing $H \to cB$.

[16] J. D. Jackson, *Classical Electrodynamics*, 3rd ed. (John Wiley and Sons, New York, 1999), Chap. 11.

[17] V. P. Gusynin, S. G. Sharapov, and J. P. Carbotte, Int. J. Mod. Phys. B **21**, 4611 (2007).

[18] B. Hunt, J. D. Sanchez-Yamagishi, A. F. Young, M. Yankowitz, B. J. LeRoy, K. Watanabe, T. Taniguchi, P. Moon, M. Koshino, P. Jarillo-Herrero, and R. C. Ashoori, Science **340**, 1427 (2013).

[19] R. V. Gorbachev, J. C. W. Song, G. L. Yu, A. V. Kretinin, F. Withers, Y. Cao, A. Mishchenko, I. V. Grigorieva, K. S. Novoselov, L. S. Levitov, and A. K. Geim, Science **346**, 448 (2014).

[20] C. R. Woods, L. Britnell, A. Eckmann, R. S. Ma, J. C. Lu, H. M. Guo, X. Lin, G. L. Yu, Y. Cao, R. V. Gorbachev, A. V. Kretinin, J. Park, L. A. Ponomarenko, M. I. Katsnelson, Yu.N. Gornostyrev, K. Watanabe, T. Taniguchi, C. Casiraghi, H.-J. Gao, A. K. Geim *et al.*, Nat. Phys. **10**, 451 (2014).

[21] Z.-G. Chen, Z. Shi, W. Yang, X. Lu, Y. Lai, H. Yan, F. Wang, G. Zhang, and Z. Li, Nat. Commun. **5**, 4461 (2014).

[22] Note that in [26] the oposite direction of the magnetic field is chosen which results in the change of sign in the appropriate equations and in [29] another sign before e in the covariant derivative is used.

[23] A. H. MacDonald, Phys. Rev. B **28**, 2235 (1983).

[24] C.-L. Ho and V. R. Khalilov, Phys. Rev. A **61**, 032104 (2000).

[25] O. V. Gamayun, E. V. Gorbar, and V. P. Gusynin, Phys. Rev. B **83**, 235104 (2011).

[26] Y. Zhang, Y. Barlas, and K. Yang, Phys. Rev. B **85**, 165423 (2012).

[27] S. Sun and J.-L. Zhu, Phys. Rev. B **89**, 155403 (2014); R. Van Pottelberge, M. Zarenia, and F. M. Peeters, *ibid.* **97**, 207403 (2018); J.-L. Zhu, G. Li, and N. Yang, *ibid.* **97**, 207404 (2018).

[28] H. Li, H. Liu, R. Joynt, and X. C. Xie, arXiv:2109.05403.

[29] J. F. Rodriguez-Nieva and L. S. Levitov, Phys. Rev. B **94**, 235406 (2016).

[30] S. Yu. Slavyanov and W. Lay, *Special Function: A Unified Theory Based on Singularities* (Oxford University Press, Oxford, NY, 2000).

[31] M. V. Fedoryuk, *Asymptotic Analysis: Linear Ordinary Differential Equations* (Springer, Berlin, 1993).

[32] V. Yu. Lazur, O. K. Reity, and V. V. Rubish, Theor. Math. Phys. **143**, 559 (2005).

[33] A. Kormányos, P. Rakyta, L. Oroszlany, and J. Cserti, Phys. Rev. B **78**, 045430 (2008).

[34] M. Brack and R. K. Bhaduri, *Semiclassical Physics, Frontiers in Physics*, Vol. 96 (Addison-Wesley, Reading, PA, 1997), p. 78.

[35] V. P. Gusynin and S. G. Sharapov, Phys. Rev. B **73**, 245411 (2006).

[36] H. Goldstein, C. P. Poole, and J. L. Safko, *Classical Mechanics*, 3rd ed. (Addison-Wesley, Boston, 2002).

[37] A. Bhuiyan and F. Marsiglio, Am. J. Phys. **88**, 986 (2020).

[38] C. W. Groth, M. Wimmer, A. R. Akhmerov, and X. Waintal, New J. Phys. **16**, 063065 (2014).

[39] H. B. Nielsen and M. Ninomiya, Nucl. Phys. B **185**, 20 (1981).

[40] See Supplemental Material at http://link.aps.org/supplemental/10.1103/PhysRevB.106.085401 for more detailed evolution of energy levels as a function of β with changing the value of the gap δ.

[41] Y. Zeng, J. I. A. Li, S. A. Dietrich, O. M. Ghosh, K. Watanabe, T. Taniguchi, J. Hone, and C. R. Dean, Phys. Rev. Lett. **122**, 137701 (2019).

[42] G. Li and E. Y. Andrei, Nat. Phys. **3**, 623 (2007); G. Li, A. Luican, and E. Y. Andrei, Phys. Rev. Lett. **102**, 176804 (2009).

[43] E. V. Castro, M. A. Cazalilla, and M. A. H. Vozmediano, Phys. Rev. B **96**, 241405(R) (2017).

[44] D. Grassano, M. D'Alessandro, O. Pulci, S. G. Sharapov, V. P. Gusynin, and A. A. Varlamov, Phys. Rev. B **101**, 245115 (2020).

[45] Yu. Yerin, V. P. Gusynin, S. G. Sharapov, and A. A. Varlamov, Phys. Rev. B **104**, 075415 (2021).

[46] H. Bateman and A. Erdélyi, *Higher Transcendental Functions* (McGraw-Hill, New York, 1953), Vol. 2.

[47] I. S. Gradshtein and I. M. Ryzhik, *Table of Integrals, Series, and Products*, 5th ed. (Academic Press, New York, 1994).

[48] V. Yu. Lazur, O. K. Reity, and V. V. Rubish, Theor. Math. Phys. **155**, 825 (2008); Phys. Rev. D **83**, 076003 (2011).

[49] F. W. Olver, D. W. Lozier, R. F. Boisvert, and C. W. Clark, *NIST Handbook of Mathematical Functions Hardback and CD-ROM by National Institute of Standards and Technology (U.S.)* (Cambridge University Press, New York, 2010).

[50] W. H. Press, S. A. Teukolsky, W. T. Vetterling, and B. P. Flannery, *Numerical Recipes: The Art of Scientific Computing*, 3rd ed. (Cambridge University Press, New York, 2007), p. 955